TOWARDS COUPLING THREE DIMENSIONAL EDDY RESOLVING GENERAL CIRCULATION AND BIOCHEMICAL MODELS IN THE BLACK SEA

TEMEL OĞUZ[1], PAOLA MALANOTTE-RIZZOLI[2], HUGH DUCKLOW[3]

[1] *Institute of Marine Sciences, Middle East Technical University, Erdemli, TURKEY*
[2] *Department of Earth, Planetary and Atmospheric Sciences, Massachusetts Institute of Technology, Cambridge, USA*
[3] *Virginia Institute of Marine Sciences, The College of William and Mary, Gloucester Point, VA, USA*

Abstract. An overview of our ongoing efforts on modeling the Black Sea general circulation and lower trophic level pelagic food web is presented. Using an eddy resolving ocean circulation model endowed with active thermodynamics and turbulence closure parameterization, a synthesis of the yearly mean and monthly varying circulations driven by the climatological wind stress, air-sea thermohaline fluxes and lateral buoyancy fluxes is given first. The main features of the vertically resolved, three dimensional biochemical model involving interactions between the inorganic nitrogen (nitrate, ammonium), phytoplankton, herbivorous zooplankton and bacterial biomasses, detritus and dissolved organic nitrogen are then described. A simplified version (depth and time) of the coupled physical-biochemical model without having the horizontal variabilities is applied to the central Black Sea conditions. Given a knowledge of physical forcing, solar radiation and subsurface nutrient source, the coupled model simulates main observed seasonal and vertical characteristic features such as formation of the Cold Intermediate Water mass, yearly evolution of the upper layer stratification, the annual cycle of phytoplankton production with the fall and spring blooms, the subsurface maximum layer in summer, as well as realistic patterns of bacterial biomass and particulate and dissolved organic materials.

E. Özsoy and A. Mikaelyan (eds.), Sensitivity to Change: Black Sea, Baltic Sea and North Sea, 469–485.

1. Introduction

The biogeochemical state of the Black Sea has undergone catastrophic changes within the last two-three decades. Among other reasons, the primary causes were the intense eutrophication as a result of increased antropogenic nutrient supply, and other man made activities (Mee, 1992; Bologa et al., 1995). Complementary to field observations, interdisciplinary modeling approach appears to be the proper tool to investigate the roles of major biochemical processes leading to the present state of the sea, to nowcast/forecast the system's response to various measures, and is therefore of vital importance to the success of any environmental management plan. Some objectives of the basinwide coupled physical-biochemical models are (i) to determine pathways of nutrient transport and how they correlate with productivity on the regional scale, (ii) to examine the influence of changes in the nutrient influx rates on the productivity and biomass distribitions in the northwestern shelf and nearby parts of the deep basin, (iii) to describe exchange of nutrients and biogenic materials between the shelf and the interior by a variety of physical processes responsible cross-shelf exchanges (iv) to describe large scale patchiness of chlorophyll concentrations in relation with large scale general circulation modulated by mesoscale motions.

The fundamental dynamics which need to be incorporated in such interdisciplinary models involve biogenic element cycling, pelagic and benthic ecosystems carbon and energy flows, as well as their coupling to the physical circulation, horizontal/vertical transport mechanisms. Even a very modest idealization of this highly nonlinear, complex system is, however, an extremely challenging task. The models should necessarily be four dimensional to incorporate mesoscale-to-gyral scale spatial variabilities, buoyancy input from major rivers, from the Bosphorus Strait and at the sea surface, topographic control of the rim current and its dynamics and instability, the coastal-deep sea interactions as well as day-to-year temporal variability. They should include different nutrients (nitrogen, phosphate, silicate, their new and recycled inorganic forms as well as dissolved and particulate organic forms) and biological groups (various size clasess of phytoplankton and zooplankton, and bacteria) in order to be able to incorporate strong regional and temporal variations of dominant planktonic species and of the nutrient limitation.

Implementation of this type of a comprehensive and interdisciplinary model should naturally follow a series of systematic exploratory studies carried out independently for both the physical and biochemical models. In the present paper, we describe our ongoing efforts leading to development of a coupled physical-biochemical model for the Black Sea. The coupled model is comprised of three interactive modules, dealing separately with

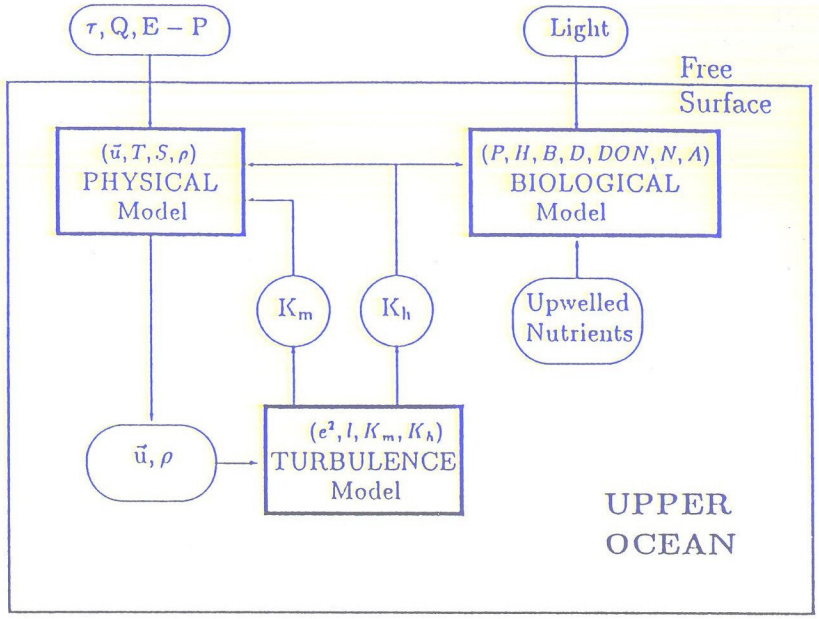

Figure 1. Schematic representation of the interactions between the physical, turbulence and biochemical modules of the interdisciplinary model.

the physical, turbulence and biological components of the system (Fig. 1). The physical module computes vertical structures of the horizontal velocity components and of density of the flow in response to wind stress, surface and lateral buoyancy forcings. The flow characteristics are then used in the turbulence module to compute the vertical eddy viscosity and diffusivity using Mellor-Yamada level 2.5 turbulence closure parameterization. The vertical turbulent diffusivity forms the main coupling of the mixed layer dynamics with the biological system. In this approach, internal structure of the physical-biological system is evolved solely in response to external forcings applied as the boundary conditions at the free surface and bottom of the ocean. This makes its main difference from the mixed layer-based biological models. In the latter type modeling approach, on the other hand, both the mixed layer structure and the interfacial mixing have to be specified a priori throughout the year.

The paper is organized as follows: In Sections 2 and 3, Numerical modeling approaches for simulation of the Black Sea general circulation and for describing the basic biochemical processes associated with the nutrient

cycling and the bacteria-plankton dynamics are presented in Sections 2 and 3, respectively. Neglecting contribution of the lateral variability in the sea for the time being, a one-dimensional application of the coupled model to the central Black Sea conditions is provided in Section 4.

2. General Characteristics of the Circulation Model

The Princeton Ocean Model of Mellor (1991) is implemented to the Black Sea configuration. It is an eddy-resolving, primitive equation model endowed with active thermodynamics, and Mellor and Yamada level 2.5 turbulence closure parameterization. The model accommodates a bottom-following σ coordinate in the vertical and a boundary fitted orthogonal curvilinear coordinate system in the horizontal. The model resolves steep topographical changes around the periphery of the basin using $O(10km)$ grid spacing and 18 vertical levels which are compressed towards the free surface to resolve the thin, $O(150m)$, upper layer of the Black Sea stratification.

Using standard climatological data sets (wind stress of Hellerman and Rosenstein [1983] and surface fluxes of Altman et al. [1987], and initializing the model with a horizontally uniform one dimensional stratification obtained by basinwide averaging of the yearly mean climatological data the individual roles of climatological forcings by the wind stress, surface thermal and salt fluxes and the lateral fresh water discharge in generating major features of the yearly mean circulation and its seasonal evolution are studied in Oguz, Malanotte-Rizzoli and Aubrey (1995) and Oguz, Malanotte-Rizzoli (1996b). The main findings from these studies are summarized below.

The model domain with orthogonal curvilinear coordinates has the average grid spacings of 8.5 km and 11.5 km in the meridional and zonal directions, respectively. The grid spacing attains a resolution of about 5 km along the Turkish coast where the topography undergoes its most pronounced variations. It increases maximally to about 15 km within the rest of the basin. Considering that the first baroclinic radius of deformation is about 20-30 km in the Black Sea, mesoscale processes are resolved reasonably well with the model grid. 18 vertical sigma levels are used to represent the vertical stratification. They are compressed towards the free surface in order to better resolve the thin upper layer stratification with about 3-to-6 kg/m^3 density changes. For example, for a water column of 2000 m depth, the upper 200 m layer has nine vertical levels.

The model experiments indicate that, under all forcing mechanisms, the overall basin circulation is characterized by a very strong seasonal cycle controlled primarily by the seasonal evolution of the surface thermohaline fluxes. The wind driven circulation possesses some sub-basin and gyral scale

structures which persists throughout the year. They are also seen in the circulation pattern driven by the annual mean wind stress. The rim current undergoes continuous evolution within the year. The cyclonic cell, covering the entire basin interior shown in the yearly mean circulation (see Fig. 10a,b in Oguz, Malanotte-Rizzoli and Aubrey, 1995) therefore exhibit a strong seasonal evolution. As a result, sub-basin scale cyclonic gyres of the interior cell interact, split and coalesce throughout the climatological year. The sub-basin scale circulation is also modulated by strong mesoscale activity leading to the formation of cyclonic/anticyclonic eddies along the peripheral current system. The intense mesoscale activity is evidently linked to the meanders and instabilities of the rim current, and reminescent of the surface patterns observed in satellite imagery. The overall wind-driven circulation seems therefore to be more strongly affected by the seasonal cycle with the exception of only a few localized structures that persists throughout the year. The monthly mean February and August circulation patterns representing, respectively, the winter and summer conditions of the wind driven motion are shown in Fig. 2a,b.

Contrary to the wind stress forcing, the horizontally varying surface flux distributions tend to generate a much simpler circulation pattern. In winter the circulation is characterized by a pair of zonally elongated basinwide cells. The northern cell is induced by the response to stronger cooling in the northern half of the basin, whereas the southern cell is developed by the dominant effect of precipitation. In summer both warming and excess of evaporation generate a basinwide anticyclonic cell. When the freshwater discharge is introduced in the northwestern shelf, the wintertime anticyclonic cell of the southern basin breakes into two separate gyres in the western and eastern basins, separated by a cyclonic gyre in between. Thus, also the circulation induced by the surface cooling alone and the surface and buoyancy forcings together exhibit a strong seasonal cycle. An important result of the purely thermally driven circulations is that the observed seasonal reversal of the coastal-deep water temperature gradients can be generated solely by the seasonal cycle of the surface thermal fluxes.

The fresh water discharge from the Danube is able to generate basinwide circulation comparable to circulation caused by the wind stress or surface fluxes. Although the freshwater input is only 10,000 m^3/sec, the buoyancy source introduces a strong baroclinic pressure gradients which eventually drive a strong depth integrated along-isobath flow under the action of jebar effect. This process ultimately give rise to a well-developed, strongly meandering Rim Current and accompanied temperature and salinity variations around the basin. Locally, the Danube inflow drives a strong anticyclonic circulation over the northwestern shelf. This cell is closed by a southwestward current flowing along the shelf break topography. The anti-

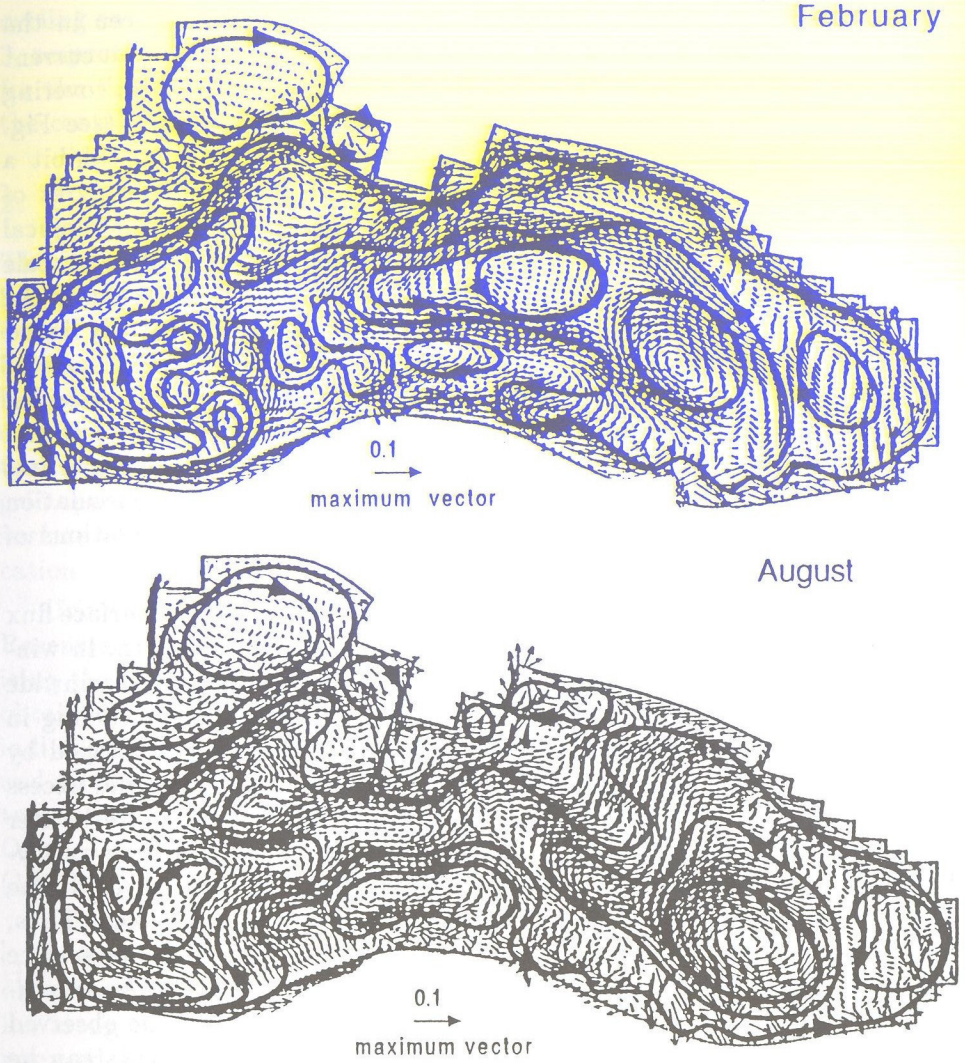

Figure 2. 5 m monthly mean wind driven circulation pattern for (a) February, (b)August. Maximum currents are scaled by 10 cm/sec for clarity of presentations. A schematic pattern of circulation is also included on the figures (after Oguz and Malanotte-Rizzoli, 1996b).

cyclonic tendency of the shelf circulation is often supported by the satellite imagery.

The wind stress and surface/lateral buoyancy forcings are all found

to be equally important in the yearly mean circulation. In the seasonal patterns the surface thermohaline fluxes, however, seem to be the dominant mechanism under the climatological data used for this study. They reduce considerably the richness in interior structures produced in the purely wind driven circulations. Topography remains a crucial factor in controlling the pattern of the rim current system, as explored previously in the yearly mean circulation studies of Oguz, Malanotte-Rizzoli and Aubrey (1995).

The regional variability of the surface forcings also affects crucially the spatial variability of the seasonal circulation. Again, as the surface wind stress pattern does not exhibit dramatic winter-to-summer changes, the horizontal variability of the surface thermohaline fluxes is the determining factor. Particularly important is the persistence of excess precipitation in the easternmost part of the basin throughout the year. This drives one of the permanent circulation features, called the Batumi eddy. Finally, the mesoscale activity associated with the peripheral current system is mostly intense along the Turkish and Caucasian coast. They are obviously linked to the dynamical instabilities of the rim current that produce strong meandering and eddy formation especially along the southern coastline.

The model circulation can be classified as a two-layer system with vertical homogeneity in each layer. In the upper layer of about 150 m, the individual forcing mechanisms contribute to the generation of the most of the known features of circulation in the sea. The Rim Current and the interior cell are the main blocks of the basin scale circulation system. The anticyclonic gyres on the northwestern shelf and the southeastern corner, as well as the cyclonic gyres of the interior cell constitute the main sub-basin scale features. A series of anticyclonic eddies confined between the coast and the meandering Rim Current zone are products of the mesoscale variability. Other mesoscale features, such as offshore filaments, dipole structures and detached eddies are originated from the evolution of propogating meanders.

The circulation in the lower layer, below 300 m depth, is separated from the upper layer by a transition zone. It is interesting to note that the lower layer circulation is always similar under all forcings. It consists of an elongated mildly meandering cyclonic cell over the flat interior of the basin. The shoreward side of the cell is covered by an anticyclonic recirculation zone which is wider and encircles the entire basin, as compared with the one in the upper layer. The transition zone reflects essentially the motion induced by the horizontal variability of the pycnocline and varies depending on the intensity and horizontal structure of the surface fluxes. The circulation below ~300 m is basically barotropic, driven by the surface elevation whose patterns are similar for all the forcings. Hence the baroclinic component of the circulation generated in response to the deformation of the pycnocline is only limited to a transitional layer immediately below the

pycnocline.

An important byproduct of this modeling study is the necessity of re-analysis of the heat flux climatology. The existing data seem to impose a too strong local cooling and/or warming which leads to inconsistency between the computed water mass characteristics and the available observations. This does not critically alter the overall upper layer circulation characteristics, but prevents reasonably realistic horizontal distributions of temperature at the near-surface levels. Another important finding of the present work is to quantify the secondary role of the NWS region in the CIW formation process. Even though the most intensified cooling and subsequent formation of coldest waters take place in the NWS, the fresh water supply from the Danube prevents the shelf waters from being dense enough to spread into the deep interior layers of the basin by crossing over the topographic slope. Thus, during moderate-to-high discharge winters, as in the present simulations, the NWS does not contribute significantly to the overall newly formed CIL.

3. The Biochemical Model

The biochemical model describing the nutrient cycling and bacteria-plankton dynamics in the Black Sea consists of interactions and transformations between phytoplankton P, herbivorous zooplankton H, bacteria B, labile pelagic detritus D, labile dissolved organic nitrogen DON, nitrate N and ammonium A. Their temporal variations are expressed by an equation of the general form

$$\frac{D\tilde{C}}{Dt} = \frac{1}{H^2}\frac{\partial}{\partial\sigma}\left[(K_b+\nu_b)\frac{\partial\tilde{C}}{\partial\sigma}\right] + \Re_c + HmnF_C \qquad (1)$$

The material derivative on the left hand side of eq. (1) is expressed as

$$\frac{D\tilde{C}}{Dt} = \frac{\partial\tilde{C}}{\partial t} + \frac{\partial}{\partial\xi}\left(\frac{u\tilde{C}}{m}\right) + \frac{\partial}{\partial\eta}\left(\frac{v\tilde{C}}{n}\right) + \frac{1}{H}\frac{\partial}{\partial\sigma}\left(\omega\tilde{C}\right) \qquad (2)$$

K_b and ν_b are the vertical eddy and molecular diffusion coefficients, respectively. They are assumed to be same with those of the heat and salt equations. F_C represents the biological interaction terms which are expressed for each of the biological variables as (e.g. Fasham et al., 1990)

$$F_P = (1-\kappa)\,\Phi_p P - G_p(P)\,H - m_p P \qquad (3)$$

$$F_H = \gamma_p G_p(P)\,H + \gamma_b G_b(B)\,H - m_h H - \mu_h H \qquad (4)$$

TABLE 1. Biological model parameters and definitions

Parameter	Definition	Value	Units
ν_b	Background (molecular) value of kinematic viscosity and diffusivity	$1\text{x}10^{-6}$	m^2s^{-1}
σ_m	Maximum phytoplankton growth rate	1.5	day^{-1}
a	Photosynthesis efficiency parameter	0.01	nondimensional
k_w	Light extinction coefficient for PAR	0.08	m^{-1}
k_c	Phytoplankton self-shading coefficient	0.07	m^2 (mmol-N)$^{-1}$
R_n	Nitrate half saturation constant	0.5	mmol-N m^{-3}
R_a	Ammonium half saturation constant	0.2	mmol-N m^{-3}
ψ	Ammonium inhibition parameter	3.0	(mmol-N)$^{-1}$
m_p	Phytoplankton death rate	0.04	day^{-1}
κ	Phytoplankton exudation fraction	0.05	nondimensional
r_g	Herbivore maximum grazing rate	0.6	day^{-1}
m_h	Herbivore death rate	0.04	day^{-1}
μ_h	Herbivore excretion rate	0.12	day^{-1}
γ_p	Herbivore assimilation efficiency	0.75	nondimensional
R_g	Herbivore grazing half saturation constant	0.5	mmol-N m^{-3}
σ_b	Maximum bacterial growth rate	0.35	day^{-1}
γ_b	Bacterial assimilation efficiency	0.7	nondimensional
r_b	Bacterial maximum grazing rate	0.25	day^{-1}
R_b	Bacterial grazing half saturation constant	0.5	mmol-N m^{-3}
μ_b	Bacteria excretion rate	0.05	day^{-1}
ϵ	Detrital remineralization rate	0.1	day^{-1}
w_s	Detrital sinking rate	2.0	m day^{-1}
Ω_n	Ammonium nitrification rate	0.5	m day^{-1}
Ω_d	nitrate denitrification rate	0.5	m day^{-1}
λ	partition of detritus between DON and Ammonium	0.5	nondimensional

$$F_D = (1-\gamma_p)\,G_p(P)\,H + (1-\gamma_b)\,G_b(B)\,H + m_p P + m_h H - \epsilon D + \frac{w_s}{H}\frac{\partial D}{\partial\sigma} \qquad (5)$$

$$F_{DON} = -\Phi_b B + \kappa\Phi_p P + \lambda\epsilon D \qquad (6)$$

$$F_B = \Phi_b B - G_b(B)\,H - \mu_b B \qquad (7)$$

$$F_A = -\sigma_m\alpha(I)\,\beta_a(A)\,P + \mu_h H + (1-\lambda)\,\epsilon D + \mu_b B - \Omega_n A \qquad (8)$$

$$F_N = -\sigma_m\alpha(I)\,\beta_n(N)\,P + \Omega_n A - \Omega_d N \qquad (9)$$

where the definition of parameters are given in Table 1.

In the phytoplankton equation, the primary production is expressed as a function of light, nitrate and ammonium uptakes by

$$\Phi_p = \sigma_m \alpha(I)\left[\beta_a(A) + \beta_n(N)\right] \tag{10}$$

The maximum specific production rate under optimum light and nutrient conditions does not have the temperature dependence. Daily variations of the photosynthetically available radiation are neglected. The losses are due to the herbivore grazing and natural mortality. The effects of respiration and phytoplankton excretion are included in the latter loss term. 5% of the total primary production is assumed to be exudated as DON.

The nutrient limitation functions for the ammonium $\beta_a(A)$ and for the nitrate $\beta_n(N)$ are expressed by the standard Michaelis-Menten formulations

$$\beta_a(A) = \frac{A}{R_a + A} \qquad \beta_n(N) = \frac{N}{R_n + N}\exp(-\psi A) \tag{11}$$

where R_n and R_a are the half-saturation constants for nitrate and ammonium, respectively. The exponential term represents the inhibiting effect of ammonium concentration on nitrate uptake, with ψ signifying the inhibition parameter. The light limitation is parameterized by

$$\alpha(I) = tanh\left[aI(z;P,t)\right] \tag{12}$$

$$I(z,P,t) = I_s \exp\left[-(k_w + k_c P)\, z\right] \tag{13}$$

where a denotes photosynthesis efficiency parameter, I_s is the surface intensity of the PAR, k_w is the light attenuation coefficient due to sea water, and k_c is the phytoplankton self-shading coefficient. The grazing rates of herbivores on phytoplankton is represented by

$$G_p(P) = r_g \frac{P}{R_g + P} \tag{14}$$

where r_g is the maximum grazing rate, and R_g denotes the half-saturation constant. A similar expression is also used to express the bacterial grazing of herbivores.

The zooplankton are fed by assimilating 70%'s of the phytoplankton and bacterial grazing. The losses are excretion and mortality. The excretion occurs in the form of ammonium. The mortality term represents dead zooplankton biomass as well as losses by higher predators which are not considered explicitely in the model. The main source of the detrital pool is the fecal pellets constituting 30%'s of the zooplankton grazing of phytoplankton and bacteria. All the phytoplankton losses and the dead zooplankton biomass constitute additional detrital sources. Detritus sink downward with

a fall speed w_s. It is assumed that only 50% of the particulate matter is converted into DON form, the rest is converted instantly into ammonium form, and does not take place in the bacterial production process.

In addition to the detrital breakdown, the other DON production mechanism is the phytoplankton exudation. The bacteria take up the DON, excrete ammonium and are grazed by zooplankton. No bacterial mortality is modeled separately; its effect is embedded in the excretion term. The bacterial uptake of the dissolved organic nitrogen is expressed by

$$\Phi_b = \sigma_b \frac{DON}{R_b + DON} \tag{15}$$

with σ_b and R_b signifying the maximum bacterial growth rate and the half saturation constant, respectively. Thus, the nitrogen requirement of the bacterial growth process is met simply by the DON, and the ammonium contribution (see Fasham et al., 1990) is not incorporated in this process.

The zooplankton and bacterial excretion as well as a part of detrital breakdown signify the three mechanisms in the ammonium equation responsible for the nitrogen cycling and the regenerated production. The ammonium consumption of the phytoplankton during the photosynthesis and nitrification process consitute the sink terms. The nitrification process is parameterized as a direct conversion of ammonium to nitrate without the intermediate level of nitrite transformation. The nitrification rate is taken vertically uniform above the depth of the 15.6 kg/m^3 sigma-t level, decreasing linearly to zero towards the depth of the 16.2 kg/m^3 sigma-t level (Ward and Kilpatrick, 1991). At deeper levels (i.e. within the anoxic layer), no nitrification takes place. But, nitrate is denitrified to N_2 at these depths.

No-flux conditions are specified for all variables both at the surface and the bottom.

4. One Dimensional Simulation with the Coupled Physical - Biochemical Model

As a step towards the three dimensional ecosystem modeling, we present here a one-dimensional version of the coupled model with no horizontal dependence. A similar model with five compartments of the biological module (without DON and bacteria) was described in Oguz et al. (1996c). This simplified approach provides a basic understanding of the first order biological processes relevant for the central Black Sea, away from the shelf and the Rim Current frontal zone.

The model is initialized with the stably stratified upper ocean temperature, salinity, nitrate and ammonium profiles representative of the autumn

conditions for the interior part of the sea. A total of 51 vertical levels is used for the water column of 200 m depth representing the upper layer of the Black Sea. The grid spacing is compressed slightly towards the surface to increase the resolution near the uppermost levels. A typical grid spacing is about 5 m, except near the boundaries. The vertical diffusion terms and some of the biological terms in each of the equations (1)-(9) are solved implicitely using a time step of 5 minutes. The physical and turbulence modules, without the biological module, is first integrated for five years until an equilibrium state is achieved with repeating yearly cycles of the physical variables. The physical model is forced by the monthly varying wind and surface heat flux climatologies given by Efimov and Timofeev (1990). The monthly surface salinity values, obtained from the climatological atlas of Altman et al. (1987), are stipulated as the boundary condition in the salinity equation. Using the fifth year's cycle of the physical-turbulence models, the biological model is then forwarded in time for four years to obtain yearly cycles in all the biological variables.

Using the parameter values given in Table 1, a simulation run describing basic features of the nitrogen cycling and bacteria-plankton dynamics in the central Black Sea are shown in Figs. 3 and 4. The temporal and vertical distributions of nitrate (Fig. 3) exhibit an almost complete depletion within the shallow surface mixed layer during the period from May to November. The lack of vertical mixing across the sharp thermocline leads to consumption of the entire nitrate stocks within the mixed layer during the summer. This layer is separated from the waters having relatively richer nitrate concentrations by a seasonal nutricline confined between the depths of 20-to-30 m. It is only after November, once the seasonal thermocline is eroded, the surface layer begins to accumulate nitrate by entrainment from nitrogen-rich subsurface waters. The entire convectively generated mixed layer of about 50 m thus attains a vertically uniform nitrate concentrations during the winter period. The winter mixed layer is separated from the subsurface nitrate maximum zone by a strong permanent nutricline centered approximately at 60 m. In the rest of the year, when the mixed layer is much shallower, the layer bounded by the permanent and seasonal nutriclines signifies the biochemically active zone of nitrification process. Consequently, this layer exhibits more uniform variations between the depleted surface waters and subsurface nitrate maximum. At depths below the maximum, nitrate concentrations does not change much as compared with the initial profile. It tends to zero at a depth of about 120 m corresponding here to the level of oxic/anoxic interface.

The phytoplankton distribution (Fig. 4a) reveals a major peak during March with concentrations of 1.8 mmolN/m^3 within the upper 30 m layer, decreasing gradually towards the base of the euphotic zone at 50m. The

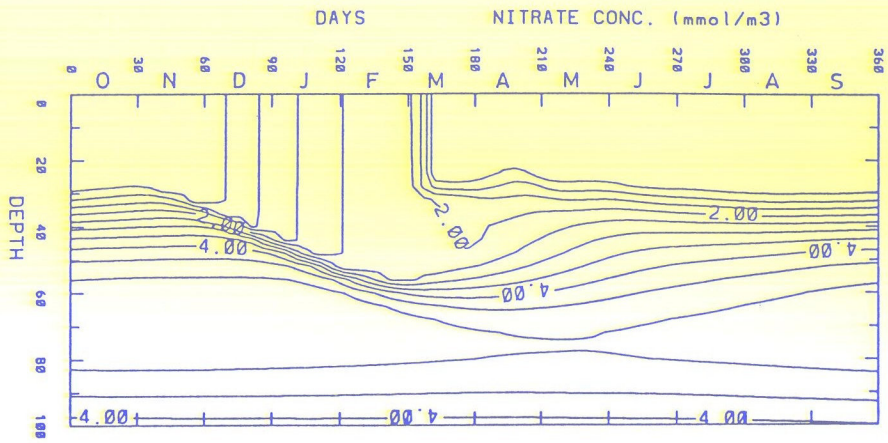

Figure 3. Depth and time variations of the nitrate concentrations computed by the one-dimensional coupled model. Day zero corresponds to the begining of October.

early spring bloom of approximately two weeks duration is followed by a shorter secondary bloom event during the third week of April. Contrary to the March bloom, the latter is related with the regenerated production due to the excess of ammonium (Fig. 4b) produced in the water column following the March bloom due to the remineralization process. In summer, a relatively weaker subsurface phytoplankton production exists below the seasonal nutricline where, in addition to nitrate, there is enough solar radiation to trigger the primary production. The summertime subsurface production is eventually combined with the surface production during November, once the atmospheric cooling starts to generate sufficiently strong vertical mixing. This is however a weaker bloom as compared with those reported by the observations. Because the model considers the vertical mixing due only to the atmospheric cooling, and does not incorporate strong short term wind induced mixing events which are very common during late autumn and early winter seasons.

All the three phytoplankton bloom events are followed by the specific periods of high zooplankton production with a time lag of about two-to- three weeks (Fig. 4c). The peak herbivore concentration is about 1.0 mmol N/m^3 occuring within the last week of March. In April, its concentration is about 0.5 mmolN/m^3 and approximately 0.20 mmolN/m^3 in November. The winter season is completely inactive in terms of plankton production. Both

phytoplankton and herbivore concentrations are almost zero in the period between the autumn and early spring blooms. While the herbivore concentrations decrease gradually inside the surface mixed layer during the summer, there exists subsurface concentrations of the order of 0.40 mmolN/m^3 within the late spring and entire summer period. The zooplankton community in the model is concentrated within the euphotic zone within the upper 50 m layer since they are grazed primarily by phytoplanktons.

The detritus distribution (not shown) exhibits its most dense concentrations of about 0.6 mmol N/m^3 right after the March bloom. Concentrations gradually reduce towards summer as they partially sink to deeper levels and, at the same time, are continually converted to dissolved organic nitrogen and ammonium forms. The DON reveals maximum concentrations during late spring and summer seasons. The peak values of about 1.0 mmolN/m^3 occurs near the surface during May, decreasing to about 0.25 mmolN/m^3 during the summer. June corresponds to the period with most drastic DON variations due to its consumption in the bacterial production process. The bacteria concentration reaches a value of 0.6 mmolN/m^3 in this month. The bacteria population is of the order of 0.1 mmolN/m^3 within the rest of the year.

4.1. MODEL-DATA COMPARISON

The nitrogen deficiency of surface waters during the summer season is supported by the nitrate measurements (Codispoti et al., 1991; Basturk et al. 1994). To our knowledge, there are not much nutrient measurements performed within the interior part of the sea during the late autumn and winter periods. The systematic measurements carried out outside the northern exit of the Bosphorus Strait (see Fig. 4 in Polat and Tugrul, 1995), on the other hand, reveal an almost one order of magnitude changes in the nitrate concentrations within the year. The mixed layer averaged concentrations of less than 0.1-0.2 mmolN/m^3 in the August-October period increase to about 2.5 mmolN/m^3 during winter, and then decrease sharply towards the summer values in spring, following the bloom event. The model results are consistent with these variations.

When the computed phytoplankton distributions is compared with the observed Chlorophyll-a distributions (see Fig. 2b in Oguz et al. 1996c), it is shown that the model is able to reproduce the two major peaks during early spring and late autumn, as well as the subsurface maximum layer during the summer period. The layer averaged peak concentration of about 1.5 mgChl-a/m^3 agrees fairly well with the data. The typical post-bloom and early summer values computed by the model is about 0.1-0.2 mgChl-a/m^3 whereas the data suggest slightly higher values of 0.3-0.4 mgChl-a/m^3 at the

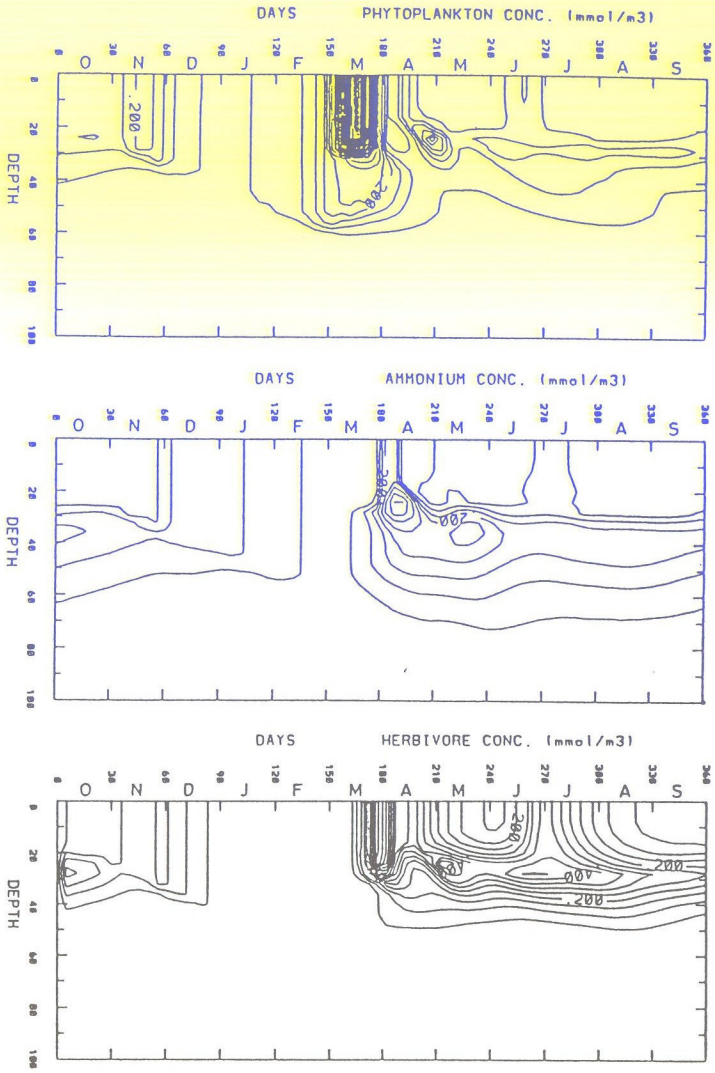

Figure 4. Depth and time variations of (a) phytoplankton, (b) ammonium, (c) zooplankton concentrations. Day zero corresponds to the begining of October.

same period. The model, on the other hand, underestimates intensity of the autumn bloom. The computed values of 0.2-0.3 mgChl-a/m^3 are lower than the observations which suggests a range of variations between 0.4 and 1.0 mgChl-a/m^3, depending on the location and the year. As we have already

emphasized above, incorporation of strong wind-induced mixing events on weekly time scales may provide a better model-data agreement.

The euphotic layer integrated peak herbivore concentration in the model amounts to ~25 mmolN/m^2 (≃2.5gC/m^2) at the begining of April, decreasing to the values of about 1.0 gC/m^2 later in the summer season, and to about 0.5 gC/m^2 during the autumn period. These values are consistent with the estimates of the mesozooplankton biomass as reported by Vinogradov (1992). The detritus exhibits similar distribution within the year. The total PON content (the sum of phytoplankton, zooplankton and detritus) within the euphotic layer are about 3.5 mmolN/m^3 during March-April period, decreasing to the values of about 2.0 mmolN/m^3 during summer months. These values are comparable with the PON values measured in the Bosphorus exit region (Polat and Tugrul, 1995).

It is difficult to compare the DON concentrations with the available observations, because of the wide range of discrepencies reported in the measured DOC values. According to data shown in Polat and Tugrul (1995), DON concentrations within the euphotic layer varies between 15 and 20 mmolN/m^3 within the year with slightly higher values in the summer months and lower ones during the winter months. If the labile fraction of DON is assumed to be around 5% of the total, then the measured labile DON concentrations should be about 0.75-1.0 mmolN/m^3. Our computed DON values are in good agreement with this estimate. The bacterial biomass has the summer peak value of 0.4 mgC/m^3 during June. The average concentration within the euphotic layer is about 0.2 mgC/m^3 in spring season, and around 0.10 mgC/m^3 within the late summer and autumn season. These are the typical range of variations in the photoautotrophic bacterial biomass concentrations as suggested by the observations (Sorokin, 1983).

5. Acknowledgements

This work was supported in part by TU-Black Sea Project sponsored by the NATO Science for Stability Program, in part by the National Science Foundation, Grant No: INT.9310226 and the Office of Naval Research, Grant No: N00014-95-1-0226. Under these grants, Temel Oguz was visiting scientist at MIT-USA during June 1993-July 1994 and June-July-August 1995.

References

1. Altman, E.N., I.F. Gertman, Z.A. Golubeva (1987) *Climatological fields of salinity and temperature in the Black Sea.* State Oceanographical Institute, Sevastopol Branch, 109pp (in Russian).
2. Basturk, O., C. Saydam, I. Salihoglu, L.V. Eremeeva, S.K. Konovalov, A. Stoyanov, A. Dimitrov, A. Cociasu, L. Dorogan, M. Altabet (1994) Vertical variations in the principle chemical properties of the Black Sea in the autumn of 1991. *J. Marine Chemistry*, **45**, 149-165.
3. Bologa, A.S., N. Bodeanu, A. Petran, V. Tiganus, Yu. P. Zaitsev (1995) *Major modifications of the Black Sea benthic and planktonic biota in the last three decades.* In: Mediterranean tributary Seas, CIESM Science Series No 1, Ed. Frederic Briand, Monaco, Musee Oceanographique, pp.85-110.
4. Codispoti,L.A., G.E. Friederich, J.W. Murray, C.M. Sakamoto (1991) Chemical variability in the Black Sea: implications of continuous vertical profiles that penetrated the oxic/anoxic interface. *Deep Sea Res.*, **38**, Suppl.2, S691-S710.
5. Efimov, V.V., and N.A. Timofeev (1990) *Investigation of the Black Sea and Azov Sea heat balance.* Technical Report, Ukranian Academy of Sciences, Sevastopol, 237pp.
6. Fasham, M.J.R., H.W. Ducklow, S.M. McKelvie (1990) A nitrogen-based model of plankton dynamics in the oceanic mixed layer. *J. Mar. Res.*, **48**, 591-639.
7. Hellermann, S. and M. Rosenstein (1983) Normal monthly wind stress over the world ocean with error estimates. *J. Phys. Oceanogr.*, **13**, 1093-1104.
8. Mee, L.D. (1992) The Black Sea in crisis: The need for concerted international action.*Ambio*, **21**, 278-286.
9. Mellor, G.L. (1991) *User's guide for a three dimensional, primitive equation, numerical ocean model.* Prog. in Atmos. and Ocean. Sci., Princeton University, 35pp.
10. Oguz, T., V.S. Latun, M.A. Latif, V.V. Vladimirov, H. I. Sur, A.A. Markov, E. Ozsoy, B.B. Kotovshchikov, V.V. Eremeev, U. Unluata (1993) Circulation in the surface and intermediate layers of the Black Sea. *Deep Sea Res. I*, **40**, 1597-1612.
11. Oguz, T., D.G. Aubrey, V.S. Latun, E. Demirov, L. Koveshnikov, V. Diacanu, H.I. Sur, S. Besiktepe, M. Duman, R. Limeburner, V. Eremeev (1994) Mesoscale circulation and thermohaline structure of the Black Sea observed during HydroBlack'91. *Deep Sea Research I*, **41**, 603-628.
12. Oguz, T., P. Malanotte-Rizzoli, D. Aubrey (1995) Wind and thermohaline circulation of the Black Sea driven by yearly mean climatological forcing. *J. Geophys. Res.*, **100**, 6845-6863.
13. Oguz, T., D. Aubrey, S. Besiktepe, L. Ivanov, V. Diacanu, U. Unluata (1996a) ADCP observations of the western Black Sea Rim Current. *to appear in Deep Sea Res.*
14. Oguz, T. and P. Malanotte-Rizzoli (1996b) Seasonal variability of wind and thermohaline driven circulation in the Black Sea. *J. Geophys. Res.*, **101**(C7), 16585-16599.
15. Oguz, T., H. Ducklow, P. Malanotte-Rizzoli, S. Tugrul, N. P. Nezlin, U. Unluata (1996c) Simulation of annual plankton productivity cycle in the Black Sea by a one-dimensional physical-biological model. *J. Geophys. Res.*, **101**(C7), 16551-16569.
16. Oguz, T., L.I. Ivanov, S. Besiktepe, E. Demirov, V. Diacanu, A.V. Grigorev, M. Duman, D.G. Aubrey (1996d) Kinematical description of basinwide circulation and thermohaline characteristics of the Black Sea during July 1992. *Submitted to J. Marine Systems.*
17. Polat, S.C. and S. Tugrul (1995) Nutrient and organic carbon exchanges between the Black and Marmara Seas through the Bosphorus Strait. *Cont. Shelf Res.*, **15**, 1115-1132.
18. Vinogradov, M.E. (1992) *Long-term variability of the pelagic community structure in the open part of the Black Sea.* In: Problems of the Black Sea. Proc. International Conference, Sevastopol, Ukraine. November 10-15, 1992. MHI-UAS Publication, pp.19-33.
19. Ward, B.B. and K.A. Kilpatrick (1991) *Nitrogen transformations in the oxic layer of permanent anoxic basins: The Black Sea and Cariaco Trench.* In: Black Sea Oceanography, NATO ASI Series C-Vol.351, E.Izdar and J.W. Murray, editors, Kluwer Academic Publishers, Dordrecht, pp.111-124.